Wide-Locking Bandwidth Optically Injection-Locked Oscillators: S-Parameter Design and Modulation Effects

Dirk Sommer and Nathan J. Gomes, *Member, IEEE*

***Abstract*—An S-parameter design approach for optically injection-locked microwave oscillators is presented. The approach is verified through the design of a 2.1-GHz microstrip MESFET oscillator that is locked by the detected signal from an edge-coupled heterojunction phototransistor. Relative locking bandwidths (B/f_0) of over 10% have been measured. The effects of modulated locking signals on such wide locking bandwidth oscillators are also considered, and it is shown that they may be used as FM transmitters and as AM-to-PM converters.**

I. Introduction

THE OPTICAL injection locking of microwave oscillators has applications in optically fed wireless communication networks and in complex microwave systems. In optically fed wireless local-area networks (LAN's) [1] or personal communications networks (PCN's) [2], [3], an optical fiber backbone can be used to synchronize base station transceivers. In complex microwave systems, such as array antennas where multiple oscillators need to be synchronized, optical fiber signal distribution can lead to significant advantages in weight/bulk and cost savings and in immunity to interference. Many optical techniques for beamforming in phased arrays have also been proposed [4], [5].

Two categories of optically injection-locked oscillators can be defined: those employing direct optical injection locking and those employing indirect optical injection locking. With direct optical injection locking, the microwave-modulated optical source is used to illuminate the active oscillator device itself. With indirect optical injection locking a photodetector is employed to convert the microwave modulation on the optical carrier to an electrical signal, which is then injected into the oscillator. The insertion of amplification and buffering stages between the photodetector and oscillator would enable the optimization of the locking signal level and allow isolation of the photodetector from the oscillator circuit, but at the expense of a considerable increase in complexity. As the locking problem would also be reduced virtually to that of an electrically locked oscillator, in most cases, the term optical injection locking has been reserved to configurations of the two preceding types (that is, without intermediate stages) [6]–[10]. Phase shifting [11] and phase modulation [12] of optically injection-locked oscillators have also been demonstrated. In [9] intensity-modulated optical signals were used to frequency modulate (at lower modulation frequencies) or lock a resonant tunnel diode oscillator. Separate optical frequency/phase control and locking have also been demonstrated within a feedback loop [13].

Injection-locked oscillators with wide locking bandwidths would be attractive in systems where it is necessary to vary the frequency of the synchronized oscillators. If the locking bandwidth were sufficiently wide it may also be feasible for the oscillators to maintain lock to a frequency modulated locking signal, allowing the oscillators to be used as FM transmitters. Thus, the optical backbone in a wireless network could distribute information-carrying microwave signals directly to base station transceiver oscillators.

In this paper, an S-parameter design approach for wide-locking bandwidth injection-locked oscillators is described (Section II). The approach is based on Adler's original theory [14] for injection-locked oscillators, suitably modified for microwave design (of reflection-type oscillators). The aim of the approach in Section II is to derive a figure-of-merit that can be optimized for design purposes. In Section III the approach is applied to the design of a 2.1-GHz indirectly optically injection-locked microstrip MESFET oscillator that uses an edge-coupled heterojunction phototransistor (HPT) as the photodetector. Results presented in Section IV demonstrate the validity of the approach for designing wide-locking bandwidth microwave oscillators. In Section V effects with modulated locking signals are described that demonstrate the use of such oscillators as FM transmitters and as AM-to-PM converters. Finally, conclusions to be drawn from the work are presented in Section VI.

II. Theory

A. Locking Bandwidth

A theoretical analysis of injection-locked oscillators was first presented by Adler [14]. The theory relies on the fact that the beating that would occur between the impressed signal and the free-running oscillation in the oscillator if it were behaving as a linear system is suppressed due to the oscillator actually operating in a nonlinear, self-limiting mode. In its locked mode the oscillator frequency shifts to that of the impressed signal. This will occur only if the oscillator's reaction time, T_R, that is the time required for the oscillation to build up, is short

Manuscript received July 19, 1994; revised December 14, 1994.

The authors are with the Optical Communications Group, University of Kent, Canterbury, Kent CT2 7NT, UK.

IEEE Log Number 9412043.

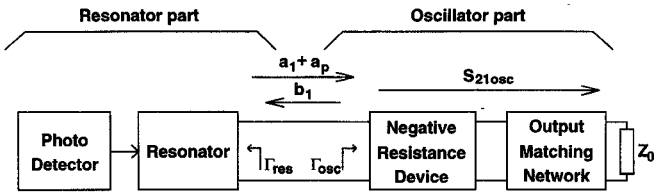

Fig. 1. General topology of oscillator circuit with indirect optical injection locking.

compared to a period of the beat frequency. Then, providing that the passband of the resonator is wide in comparison, Adler shows that the *maximum frequency deviation* $\Delta\omega_{\max}$ from the free-running frequency ω_0 within which the oscillator remains locked is given by

$$\Delta\omega_{\max} = \pm\frac{A_1}{A_0\left.\frac{d\Phi}{d\omega}\right|_{\omega=\omega_0}} \tag{1}$$

where A_1 is the amplitude of the impressed signal, A_0 is the amplitude of the oscillation (at the point of impression), and $d\Phi/d\omega|_{\omega=\omega_0}$ is the differential phase slope of the resonator. It is assumed that $A_1 \ll A_0$.

The locking bandwidth B is then simply defined as

$$B = 2\frac{\Delta\omega_{\max}}{2\pi}. \tag{2}$$

In the following derivation, Adler's theory has been redefined in terms of waves and scattering parameters to make it more relevant to the microwave design of relection-type oscillators.

The general topology for the overall injection-locked oscillator circuit is shown in Fig. 1. It is divided into an "oscillator" or active part, consisting of the negative resistance device (e.g., MESFET), and the output matching network, as well as a "resonator" part that includes the locking signal input. This division of the oscillator into two parts is the usual design approach for microwave oscillators [15] and leads to the well-known condition for oscillation, defined in terms of the reflection coefficients

$$\Gamma_{\text{osc}}\Gamma_{\text{res}} = 1. \tag{3}$$

The oscillation frequency is determined mainly by the phase condition of (3)

$$\arg(\Gamma_{\text{osc}}) = -\arg(\Gamma_{\text{res}}). \tag{4}$$

The effect of the locking signal is then analyzed by assuming it causes an additional incident wave, a_p, to arrive at the input of the oscillator part. This incident wave, a_p, adds to the incident wave $a_1 = \Gamma_{\text{res}}b_1$ that would normally occur in the manner depicted in Fig. 2. If the oscillator is locked the frequencies of a_p and a_1 are the same. Then, for analytical purposes, the effect of a_p can be considered as a change in the reflection coefficient of the resonator part to a modified value $\Gamma'_{\text{res}} = \Gamma_{\text{res}} + a_p/b_1$.

In Fig. 2 the phase difference between a_p and a_1 is shown as 90°. This is not necessarily the case as the phase difference adjusts in order to maintain lock; for example, if the locking signal was at the same frequency as the free-running

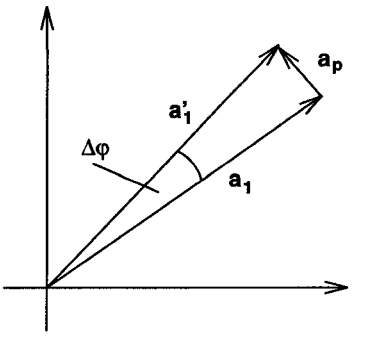

Fig. 2. Superimposing of injected signal and reflected signal from the resonator. The signal a'_1 is the total incident wave reaching the oscillator part. The diagram is the same as Adler's for the grid voltage but in terms of waves to make it applicable to a microwave circuit. If the oscillator is locked, $\Delta\varphi$ remains constant. As $|a_p| \ll |a_1|$ is assumed, $\Delta\varphi$ is in reality much smaller than depicted above.

oscillation, then the phase of Γ_{res} must be unchanged and the vectors a_p, a_1 and a'_1 would be in parallel and $\Delta\varphi$ (the phase shift) would be zero. Considering a phase difference of 90°, however, will give the maximum phase shift of Γ_{res} and will thus indicate the maximum locking bandwidth. With the assumption that the locking signal a_p is small compared to a_1, the maximum effective phase shift $\Delta\varphi_{\max}$ of Γ_{res} is

$$\Delta\varphi_{\max} \approx \left|\frac{a_p}{a_1}\right|. \tag{5}$$

This phase shift must compensate for the actual phase change with frequency of Γ_{res} and of Γ_{osc} in order that the phase condition for oscillation (4) is still met. If these phase changes are approximated linearly in the vicinity of ω_0, then

$$\Delta\varphi_{\max} = \left.\frac{d(\arg(\Gamma_{\text{res}}))}{d\omega}\right|_{\omega=\omega_0}\Delta\omega_{\max} + \left.\frac{d(\arg(\Gamma_{\text{osc}}))}{d\omega}\right|_{\omega=\omega_0}\Delta\omega_{\max}. \tag{6}$$

Rearranging the above equation for the maximum deviation $\Delta\omega_{\max}$ from the free-running frequency ω_0, using (5), one obtains

$$\Delta\omega_{\max} = \frac{|a_p|}{\left|a_1\left(\left.\frac{d(\arg(\Gamma_{\text{res}}))}{d\omega}\right|_{\omega=\omega_0} + \left.\frac{d(\arg(\Gamma_{\text{osc}}))}{d\omega}\right|_{\omega=\omega_0}\right)\right|}. \tag{7}$$

This result is directly comparable to Adler's, as given in (1). Apart from the fact that (7) is expressed in wave terminology, the major modification is the inclusion of the second term in the denominator that represents the phase slope of the oscillator (or negative resistance) part of the circuit. This was not mentioned by Adler as it is usually negligible compared to the phase slope of the resonator for typical (high-Q) oscillators. Our later design work has confirmed the necessity of this term for wide-locking bandwidth oscillators.

Finally, using (2) and writing the output power as

$$P_o = |S_{21\text{osc}}a_1|^2 \tag{8}$$

where $S_{21\text{osc}}$ is the overall forward transmission coefficient of the oscillator part and where it is assumed that $|a_1| \approx |a_1'|$ as $|a_p|$ is small, the locking bandwidth B can be expressed as

$$B = \frac{|a_p S_{21\text{osc}}|}{\left|\pi\sqrt{P_o}\left(\left.\frac{d(\arg(\Gamma_{\text{res}}))}{d\omega}\right|_{\omega=\omega_0} + \left.\frac{d(\arg(\Gamma_{\text{osc}}))}{d\omega}\right|_{\omega=\omega_0}\right)\right|}. \tag{9}$$

In deriving the above, however, it has been assumed that the oscillator part's reflection coefficient limits due to nonlinear effects so that the condition of (3) remains fulfilled, whereas all of the other parameters remain unaffected. This is not, of course, true and a reduction in $|S_{21\text{osc}}|$ particularly can be expected. Equation (9) can therefore be regarded as an upper bound on the expected locking bandwidth.

B. Figure-of-Merit

For the purposes of design it is useful to define a figure-of-merit that can be optimized. For an optically injection-locked oscillator such a figure-of-merit would incorporate the relative locking bandwidth, the oscillator output power, and the injected photocurrent. Cochran and Wang [16] have used these parameters to define a figure-of-merit γ, which can be written as

$$\gamma = \frac{B}{f_0}\frac{\sqrt{P_o}}{i_{ph}} \tag{10}$$

where i_{ph} is the peak value of the impressed photocurrent. The photocurrent generated by the photodetector should be injected somewhere into the resonator part. It will have a much more significant effect on the oscillator at this port as the "oscillator part" will provide gain; the amplitude of the injected locking signal will thus be greater relative to the oscillation at this port of the oscillator [16]. As the resonator (excluding the photodetector) is passive, the photocurrent will create an incident wave a_p according to

$$a_p = k_1 i_{ph} \tag{11}$$

where k_1 is a complex constant of unit $\Omega^{1/2}$.

It should also be remarked that the properties of the photodetector must be taken into account as part of the resonator; this is especially true in the case of a phototransistor (as in the design example described later in this paper), which will typically have a much lower output impedance, and therefore greater loading effect, than a high-speed photodiode.

Using the previous derivation for locking bandwidth and (10) and (11) above, the figure-of-merit can be rewritten for a microwave design as

$$\gamma = \frac{2|k_1 S_{21\text{osc}}|}{\left|\omega_0\left(\left.\frac{d(\arg(\Gamma_{\text{res}}))}{d\omega}\right|_{\omega=\omega_0} + \left.\frac{d(\arg(\Gamma_{\text{osc}}))}{d\omega}\right|_{\omega=\omega_0}\right)\right|}. \tag{12}$$

From (12) it can be seen that the oscillator design can be optimized in two almost independent steps, corresponding to the design of each of the two parts of the oscillator as previously defined in Fig. 1.

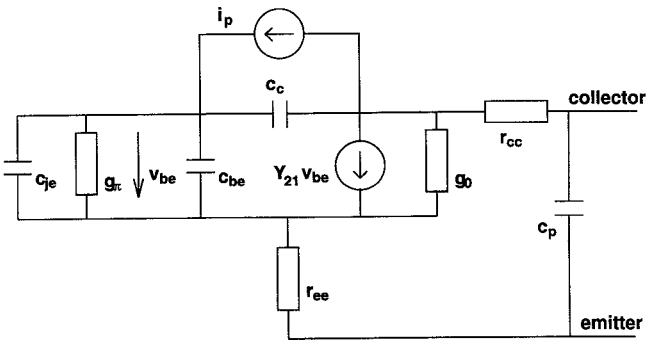

Fig. 3. Equivalent circuit model for the HPT adapted from [17] and [18] for the edge-coupled device actually used [19]. Base contact parasitics are neglected and the parasitic emitter contact pad capacitance c_p has been added. Optimized parameter values are given in the Appendix.

Step 1: An oscillator and output matching network part are designed with the objective of obtaining a high $|S_{21\text{osc}}|$ while keeping the oscillator part phase slope as small as possible.

Step 2: A resonator part is designed so that the phase condition of (4) is satisfied at the desired frequency, with the objective of obtaining a large k_1 while the resonator part phase slope is kept small.

It is, of course, important that $|\Gamma_{\text{res}}\Gamma_{\text{osc}}| > 1$ in order to ensure that oscillation starts up, and that the loading effect of the photodetector is taken into account in this, as mentioned above.

III. Design Example

In this section the theory and approach described in Section II are applied to the design of an optically injection-locked 2.1-GHz microstrip MESFET oscillator, where the locking signal is provided by an edge-coupled HPT. From previous measurements a small-signal equivalent circuit model based on the heterojunction bipolar transistor model of [17] was derived and later optimized from network analyser measurements. The major modifications to the equivalent circuit of [17] were the incorporation of a photocurrent term between collector and base [18], the neglecting of base contact parasitics due to the two-terminal nature of the device, and the addition of a parasitic capacitance between emitter and collector because of the emitter contact and bonding pad layout of the device [19]. The equivalent circuit model used for the HPT is shown in Fig. 3. Parameter values (at the most commonly used HPT bias point) are given in the Appendix.

A. Oscillator Part (Step 1)

The oscillator part should generally be kept as simple and as small as possible since large circuits will naturally involve a larger phase slope. A common-source capacitive feedback circuit employing large pads at the source connections was chosen (see Fig. 4); this circuit was optimized for an $\Gamma_{\text{osc}} > 1.5$ and an S_{21} (without matching network) as large as possible. The output matching network was then designed to increase the overall $S_{21\text{osc}}$ without introducing a large phase slope of

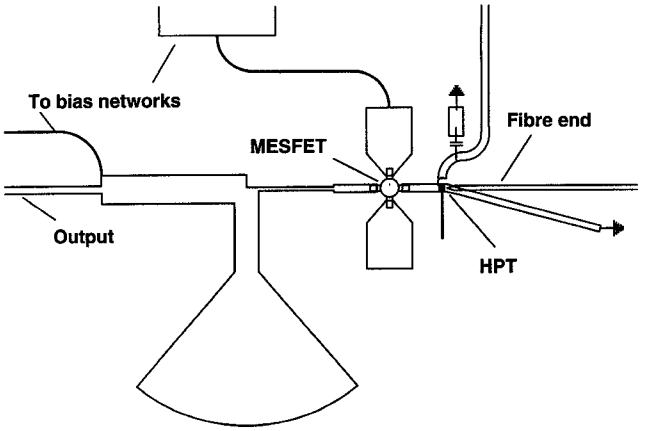

Fig. 4. Detail of the main part of the layout of the 2.1-GHz microstrip MESFET-HPT oscillator.

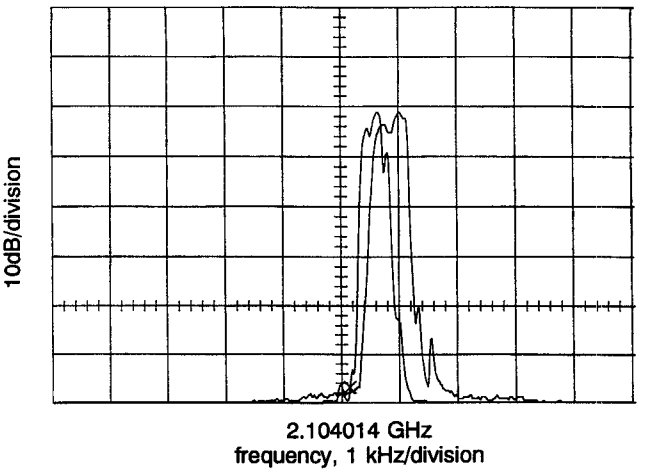

Fig. 5. Comparison of the locked oscillation spectrum with the spectrum of the locking signal (stored display, shifted left). The locking conditions were: laser RF-drive level $= -10$ dBm, $I_{CE} = 8$ mA, $I_{DS} = 10$ mA. Resolution bandwidth: 100 Hz. (The output power was uncalibrated during this measurement.)

$\Gamma_{\rm osc}$. Several structures were simulated. The one that best satisfied the design criteria consisted of a high-impedance line connected to the drain, a parallel short-circuited stub (realized by a round $\lambda/4$ stub), followed by a low-impedance line to the output. This is shown (to the left of the MESFET) in the oscillator layout of Fig. 4.

B. Resonator Part (Step 2)

A simple resonator, giving a low phase slope, would be an as-short-as-possible length of open- or short-circuited line. Simulations of the oscillator part gave a value of $\arg(\Gamma_{\rm osc})$ of approximately $-100°$. In this case, to meet the phase condition for oscillation (4), a short-circuited line of length $l < \lambda/4$ can be used. Later simulations confirmed that a short-circuited line would give better performance. The required angle of $\Gamma_{\rm res}$ (in this case 100°) is met through a choice of the line characteristic impedance and length. The phase slope of the resonator can then be found by differentiating this phase angle dependence with respect to frequency. This differentiation generally leads to the conclusion that the optimum resonator would be a very short line of high characteristic impedance, that is, as close to a perfect inductor as possible.

The second aspect of the resonator design concerns the point at which the locking signal should be injected—corresponding to the maximization of k_1 in (12). The incident wave a_p will be maximized at the oscillator if the photocurrent is impressed one-quarter wavelength away from the short-circuit at the end of the line. As it has already been stated that the total resonator length should be less than $\lambda/4$, the locking signal must be impressed as far from the short-circuit, or as close to the MESFET, as possible.

Simulations of the resonator were carried out with realistic line dimensions and these showed that results with very little deviation from the optimum could be achieved as long as $l < \lambda/8$. It should be noted that up to now the maximization of k_1 by impressing the photocurrent as close as possible to $\lambda/4$ away from the short-circuit and the minimization of the phase slope of the (passive) resonator have been assumed independent. However, the HPT has a significant effect on the resonator. For this reason the HPT model was then incorporated into the simulation to optimize the resonator line length and width.

In the oscillator circuit layout of Fig. 4 the resonator is shown to the right of the MESFET (connected to the gate terminal) with the HPT chip mounted on it close to the MESFET. The resonator has an angular deviation at the point where the HPT is attached to allow for easier optical access via an optical fiber (also illustrated in Fig. 4). The broader line above the HPT connects to the DC collector-emitter. Finally, the short, narrow stub below the HPT (in Fig. 4) was incorporated to suppress a possible resonance at 8 GHz.

IV. Locking Performance

A pig-tailed 1.3μm Fabry-Perot semiconductor laser (BT&D LSC2110) was used to illuminate the HPT. Modulated optical input was provided by driving the laser by an RF signal generator (HP 8350B/83525B) via a bias tee. Unlocked, the oscillator behavior was very noisy as it had been designed with a low-Q to facilitate locking. When locked, the phase noise decreased significantly, and as shown in Fig. 5, the spectrum of the locked oscillation compares very favorably with the locking signal. It is estimated that with the RF drive level to the laser employed to obtain the result of Fig. 5 (-10 dBm), the locking signal from the HPT is almost 50 dB lower than the oscillator output power. This has been estimated from measurements on an HPT directly connected to a spectrum analyser. The oscillator could be locked with signals from the HPT almost 70 dB lower than the oscillator output. However, at such low locking signal levels the locking bandwidth is no greater than the long-term drift of the oscillator (approximately 700 kHz), so the oscillator could drift out of the locking range, and the quality of the output spectrum deteriorated although it was still significantly better than the unlocked spectrum.

At typical bias conditions of $I_{CE} = 8$ mA and $I_{DS} = 10$ mA the locking bandwidth varied between 6.7 and 220 MHz as the RF-drive to the laser was increased from -10 to $+8$ dBm [20]. A relative locking bandwidth B/f_0 of over 10% can thus

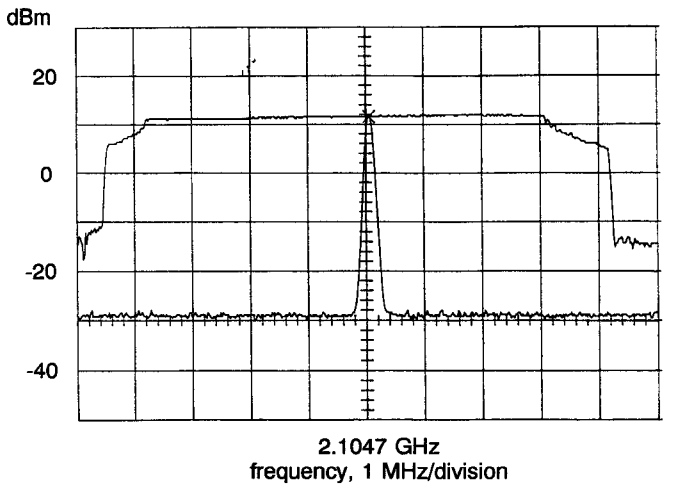

Fig. 6. Example plot of the locking bandwidth with a low-level locking signal. Locking conditions: laser RF-drive level = −10 dBm, I_{CE} = 8 mA, I_{DS} = 10 mA. Resolution bandwidth: 100 kHz.

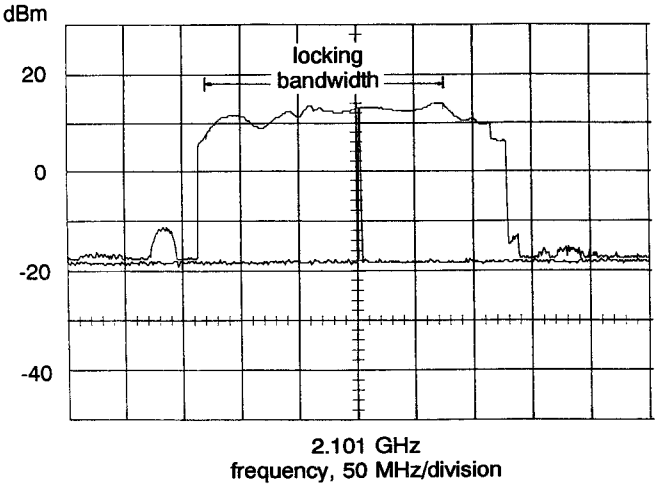

Fig. 7. Example plot of the locking bandwidth with a higher-level locking signal. Locking conditions: laser RF-drive level = +8 dBm, I_{CE} = 8 mA, I_{DS} = 10 mA. Resolution bandwidth: 1 MHz.

be achieved. Generally, however, the oscillator shows quite different behavior for low-level and high-level locking signals.

For low-level locking signals the locking bandwidth is consistent with the square-root dependence on injected power predicted by Adler [14]. The oscillator output power is nearly flat across the locking bandwidth as shown in Fig. 6. The output power drops suddenly when the locking signal moves out of the locking bandwidth and many single sidebands occur; this is typical for a driven unlocked oscillator. In this region the figure-of-merit (10) achieved is typically between 3 $\Omega^{1/2}$ and 5 $\Omega^{1/2}$.

For higher-level locking signals, that is when the locking signal level delivered by the HPT approaches and lies within approximately −35 dB of the oscillator output power (approx. 12 dBm), the locking bandwidth rises sharply. The figure-of-merit (10) achieved here is typically about 10 $\Omega^{1/2}$. However, as can be seen from Fig. 7, the oscillator output power varies by several dB across the locking bandwidth. Also, as the locking signal moves out of the locking bandwidth it merely becomes increasingly attenuated (that is, there is not a sudden drop) while the free-running oscillation reappears.

V. Modulation Performance

A. FM Transmission

With an injection-locked oscillator that remains in lock over a wide bandwidth it should be possible to vary the instantaneous frequency of the locking signal (within the locking bandwidth) and obtain a frequency-modulated output while retaining the performance advantages of locked operation. This type of operation has been previously demonstrated for electrically injection-locked oscillators [21].

Fig. 8 shows the spectra of frequency-modulated input signals with the output spectra obtained when they are injected into the HPT-MESFET oscillator. The input spectra are shifted slightly to the right of their corresponding output spectra for comparison. The modulating frequency was 1 MHz for Fig. 8(a) and 8(b). As the FM response of the signal generator was unknown, the modulation index β has been estimated from the input spectra, which indicates that $\beta = 4$. This therefore leads to a peak frequency deviation Δf of 4 MHz and a bandwidth for the instantaneous frequency of $2\Delta f = 8$ MHz.

In Fig. 8(a) the output spectrum is shown for the case where the RF-drive level to the laser is −10 dBm, which results in a locking bandwidth of 6.7 MHz (less than the bandwidth of the instantaneous frequency). The distortion of the output signal can be seen from the increased noise floor and the additional sidebands in the oscillator output spectrum. For the measurement of Fig. 8(b) the laser RF-drive level was increased to −4 dBm, which results in a locking bandwidth of 14.4 MHz. The oscillator output spectrum can now be seen to be almost the same as the input spectrum, despite the fact that some of the FM sidebands lie outside of the locking bandwidth.

The input spectra in Fig. 8 are not symmetrical, probably due to the generation of some unwanted AM in the signal generator. It is interesting to observe that the injection-locked oscillator suppresses this AM (converting it to PM—see next subsection).

The frequency modulation of the injected signal will cause an additional and varying phase shift α between the injected and locked signals and hence an additional phase modulation. This phase modulation is nonlinear ($\sin \alpha \sim \Delta\omega$, again see next subsection) and will therefore lead to some distortion if the whole of the locking range is used for the modulating signal. If only a narrower region within the locking bandwidth were used for the modulation, the additional PM could be considered approximately linear and some compensation for the phase distortion might be achieved through the use of an all-pass filter. However, it is thought that these effects need to be further investigated. FM transmission was verified as follows: Audio signals were frequency modulated onto the locking signal and the downconverted output of the oscillator was demodulated by a communications receiver (ICOM R-7000) in FM mode.

Finally, the effect of a modulating frequency greater than the locking bandwidth has been examined. The instantaneous fre-

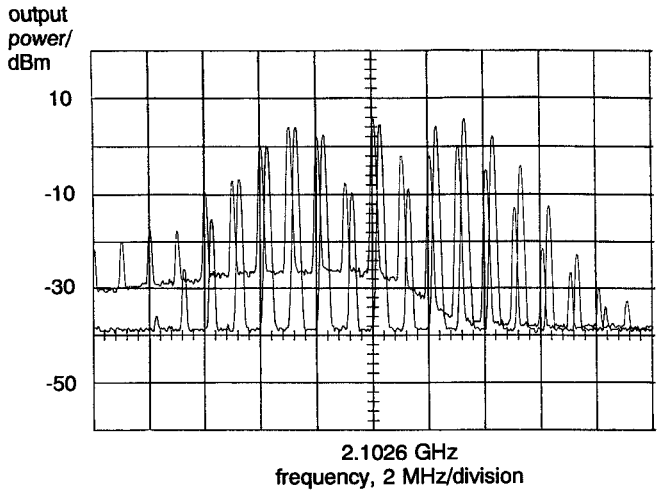

(a)

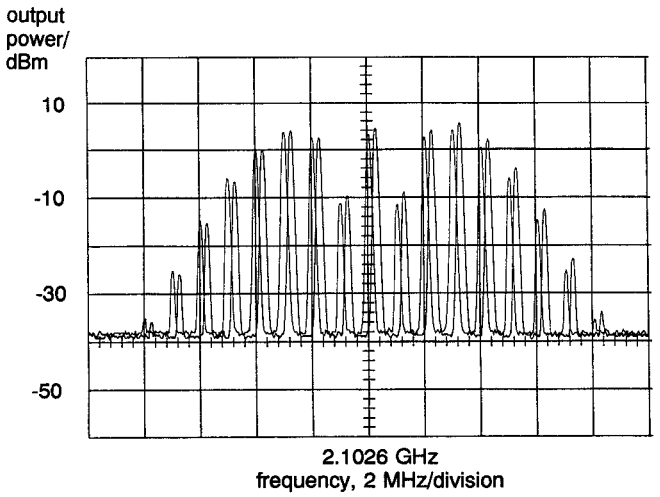

(b)

Fig. 8. Output spectra of the oscillator (left) compared to the corresponding frequency modulated locking signal spectra (right). $I_{CE} = 8$ mA, $I_{DS} = 10$ mA, $f_m = 1$ MHz, $\beta \approx 4$. (a) The maximum instantaneous frequency deviation exceeds the locking bandwidth; laser RF-drive level $= -10$ dBm, locking bandwidth $B = 6.7$ MHz. (b) The maximum instantaneous frequency deviation is within the locking bandwidth; laser RF-drive level $= -4$ dBm, locking bandwidth $B = 14.4$ MHz. Resolution bandwidth: 100 kHz.

quency was confined to the locking bandwidth by a low β but the FM sidebands (which necessarily lie outside the locking bandwidth) were considerably attenuated—by approximately 10 dB for $f_m = 10$ MHz and $B = 6.7$ MHz. However, the oscillator did not become unlocked although the input signal spectrum is considerably wider than the locking bandwidth.

B. AM-to-PM Conversion Theory

As oscillators operate in a self-limiting mode, one would not expect to observe amplitude modulation of the output when an amplitude-modulated locking signal is applied. However, as the oscillator phase will adjust itself to remain in lock for different amplitude locking signals, phase modulation would be expected. This method of direct amplitude modulation of the injected signal is different to that presented in [11] and [12], for example, where the phase shifting/modulation is caused by detuning the free-running oscillator frequency—although in the case of [12] this is achieved by varying the average incident illumination level.

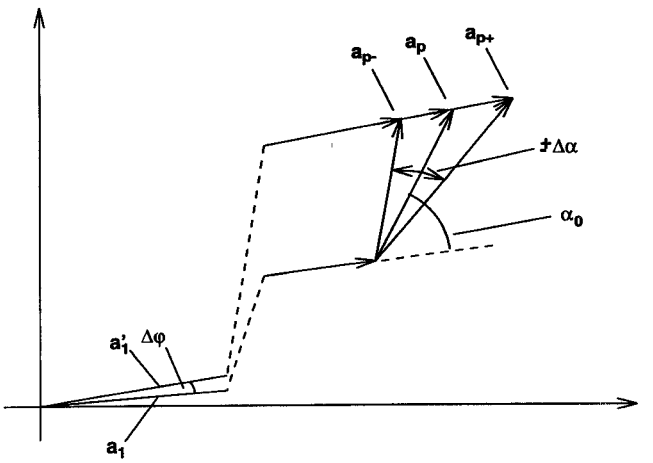

Fig. 9. Illustration of AM-to-PM conversion by the injection-locked oscillator. $\Delta\varphi$ is determined by the frequency difference $\Delta\omega$ between the free-running and injected signals. If $\Delta\varphi$ is fixed and the amplitude of the injected signal is changed, the phase difference α between the injected signal and the oscillator signal must adjust for the oscillator to maintain lock. The vector a_p is thus seen to vary between a_{p-} (diminished by the AM) and a_{p+} (enlarged by the AM).

For a simple (linearized) analytic description of the AM-to-PM conversion behavior of an injection-locked oscillator a number of assumptions need to be made.

1) The modulation index of the AM is small.
2) The phase angle $\Delta\varphi \ll 1$. This is usually the case as the maximum value for $\Delta\varphi$ (in radians) is $|a_p/a_1|$ and $a_p \ll a_1$ has been assumed. This also leads to the condition that the vectors representing a_1 and a_1' are (almost) in parallel.
3) The phase change $\Delta\varphi$ is linearly dependent on the difference $\Delta\omega$ between oscillation and free-running frequencies; this is the case if the phase slope of the resonator and oscillator parts are approximated linearly in the vicinity of ω_0, see (7).

The above assumptions are illustrated in Fig. 9. Part of the diagram is expanded to show the effect of a modulated locking signal, but the phase angle $\Delta\varphi$ is no longer exaggerated as in Fig. 2. Now, as $\Delta\varphi$ is determined by $\Delta\omega$ and is thus fixed for amplitude modulation of the impressed signal only, the phase difference between the impressed signal and the oscillator signal must adjust in order to keep the oscillator in lock. Fig. 9 shows this varying phase difference α as the impressed signal is enlarged and diminished by the AM.

The oscillator output signal $A_0(t)$ can be written as

$$A_0(t) = A\cos(\omega_1 t + \alpha_0 + \Delta\alpha(t) + \theta) \tag{13}$$

where ω_1 is the frequency of the impressed signal, θ is an arbitary phase and the phase difference between impressed signal and oscillator signal varies about α_0, so that $\alpha = \alpha_0 + \Delta\alpha(t)$. According to Adler [14] and from Fig. 9, it can be seen that

$$\sin\alpha = \left|\frac{\Delta\varphi a_1}{a_p}\right|. \tag{14}$$

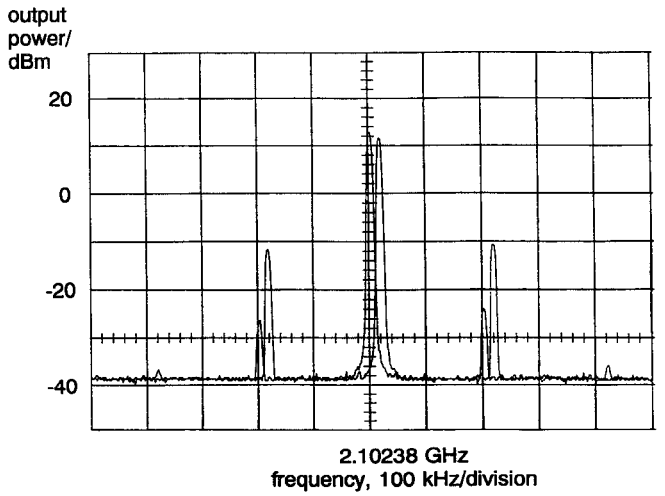

(a)

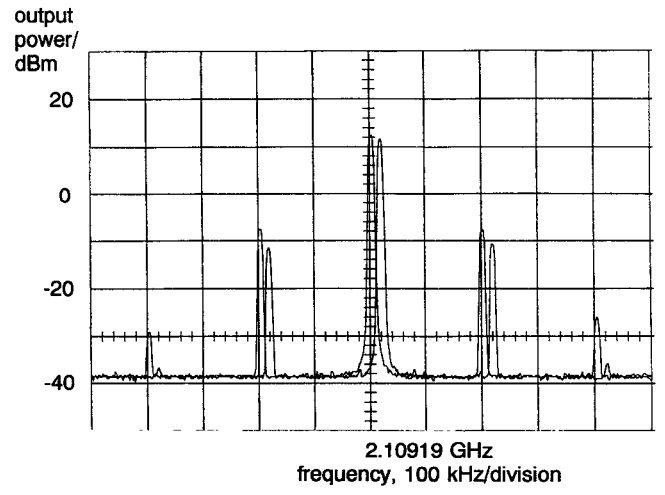

(b)

Fig. 10. Output spectra of the oscillator (left) with corresponding spectra of the amplitude modulated injected signals (right). Laser RF-drive level $= -1$ dBm, $f_m = 200$ kHz, $I_{CE} = 8$ mA, $I_{DS} = 10$ mA. (a) The injected signal frequency is equal to the oscillator free-running frequency. (b) The injected signal frequency is close to the edge of the locking bandwidth. Resolution bandwidth: 10 kHz.

If the locking signal is amplitude modulated, then it can be expressed as

$$a_p = a_{p0}(1 + m_A \cos(\omega_m t)) \tag{15}$$

where a_{p0} is the average amplitude of the locking signal, m_A is the modulation index, and ω_m is the modulation frequency in radians. Substituting (15) into (14), $\sin\alpha$ can (with a little manipulation) be expressed as

$$\sin\ \alpha \approx \left|\frac{\Delta\varphi a_1}{a_{p0}}\right|(1 - m_A \cos(\omega_m t)). \tag{16}$$

Using the Taylor series for $\sin\ \alpha$ one can write

$$\sin\ \alpha \approx \sin\ \alpha_0 + \cos\ \alpha_0 \Delta\alpha(t). \tag{17}$$

Comparing (17) and (16) one obtains

$$\sin\ \alpha_0 = \left|\frac{\Delta\varphi a_1}{a_{p0}}\right| \tag{18}$$

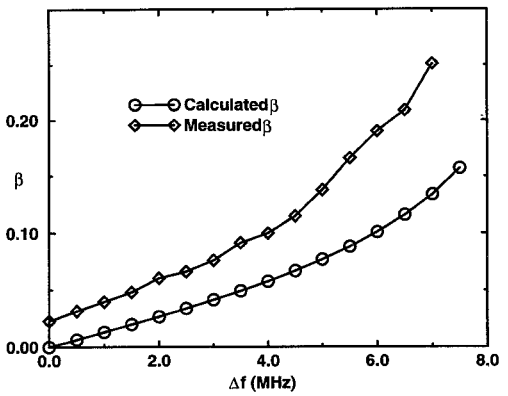

Fig. 11. Comparison of calculated and measured values of β for the phase modulation of the oscillator output caused by amplitude modulation of the injected signal, as the injected signal frequency is varied with respect to the oscillator free-running frequency.

$$\Delta\alpha(t) = -\left|\frac{\Delta\varphi\alpha_1}{\alpha_{p0}\cos\ \alpha_0}\right| m_A \cos(\omega_m t)$$
$$= -\frac{m_A \sin\ \alpha_0}{\sqrt{1 - \sin^2\ \alpha_0}} \cos(\omega_m t). \tag{19}$$

From (19) it can be seen that if the locking frequency is equal to the free-running frequency no phase modulation should be possible as both $\Delta\varphi$ and α are zero irrespective of the amplitude of the locking signal. On the other hand, if the locking frequency is near to either end of the locking bandwidth, $|\alpha_0|$ approaches 90° and the PM should increase rapidly due to the denominator of (19). Although (19) predicts that the phase deviation can become infinite, it can be expected that in reality the oscillator will become unlocked.

The amplitude of the PM sidebands can be estimated by inserting (19) into (13) and setting the arbitrary phase $\theta = -\alpha_0$ for analytical purposes, without loss of generality. Then

$$A_0(t) = A\cos\left(\omega_1 t - \frac{m_A \sin\ \alpha_0}{\sqrt{1 - \sin^2\ \alpha_0}} \cos(\omega_m t)\right). \tag{20}$$

The modulation index β is then seen to be the factor multiplying the $\cos(\omega_m t)$ term. As $\sin\ \alpha_0$ is dependent on $\Delta\varphi$, then for a linear phase slope with frequency, knowing that $\sin\ \alpha_0 = 1$ at the edge of the locking bandwidth (at $\Delta\omega_{\max}$), $\sin\ \alpha_0$ can be given by

$$\sin\ \alpha_0 = \frac{\Delta\omega}{\Delta\omega_{\max}}. \tag{21}$$

The modulation index β can then be written as

$$\beta = \frac{m_A \Delta\omega/\Delta\omega_{\max}}{\sqrt{1 - (\Delta\omega/\Delta\omega_{\max})^2}}. \tag{22}$$

C. AM-to-PM Conversion Results

Experiments were performed by amplitude modulating the locking signal to the HPT-MESFET oscillator. Fig. 10 shows results generally confirming the arguments following (19). The AM modulation index used in the experiments was $m_A =$

TABLE I

Symbol	Description of parameter	Value at I_{CE} = 8 mA
g_0	differential collector-emitter conductance	1.82 mS
g_m	transconductance	309 mS
g_π	differential base-emitter conductance	1.14 mS
c_{be}	base-emitter diffusion capacitance	4.55 pF
c_c	collector-base depletion capacitance	0.032 pF
τ_{cs}	collector-base dep. layer transit time	5.94 ps

0.13, which is probably too large for the preceding theory to be wholly accurate, but was found to be necessary to make the PM sidebands large enough for reasonable measurements. Fig. 10(a) shows the resulting output spectrum for a locking signal frequency equal to the free-running frequency; the PM sidebands are still present but are very low. In Fig. 10(b) the locking signal frequency is near to the edge of the locking bandwidth and the PM sidebands are significantly (almost 20 dB) greater. It was confirmed that the sidebands were due to angle modulation by using an audio signal to amplitude modulate the locking signal. The oscillator output was downconverted to a communications receiver band, as before. No signal was detected with the receiver switched to AM mode, whereas there was some (poor quality) reception when the receiver was in its FM mode.

The amplitudes of the first sideband of the oscillator output have been found for different $\Delta f = \Delta\omega/2\pi$. The minimum difference between the fundamental component at the injected frequency (A_{s0}) and the first sideband component (A_{s1}) was 18 dB, corresponding to a ratio $A_{s0}/A_{s1} = 0.126$. As $\beta < 0.3, \beta$ can be estimated from the measured results using $\beta = 2A_{s1}/A_{s0}$ with an error of less than 3%, which is of the same order as the measurement resolution. A comparison of the measured results for β compared to calculated values from (22) are shown in Fig. 11. It can be seen that the measured and calculated results follow the same general shape. The discrepancy between the two curves can be due to a number of factors in addition to the assumptions required in the preceding analysis. For example, instabilities in the optical setup for coupling into the HPT would cause fluctuations in $\Delta\omega_{\max}$ during the measurements, and the slight differences in levels between the two AM sidebands of the locking signal suggest that there may be some residual angle modulation. These effects would explain why the PM sidebands do not go to zero when the locking signal is tuned to the oscillator free-running frequency.

VI. Conclusion

An S-parameter design approach for wide locking bandwidth optically injection locked oscillators has been presented. The approach has been verified through its use in designing a 2.1-GHz microstrip MESFET-HPT oscillator; this oscillator has an exceptionally wide locking bandwidth (relative locking bandwidths of over 10% having been achieved). The circuit was kept in microstrip so it should be relatively straightforward to modify the design for higher frequencies. The wide-locking bandwidths achieved are due to both the high optical gain of the HPT and the optimization of the oscillator design using the developed approach.

Wide-locking bandwidth oscillators would be very useful in systems requiring the synchronization of a large number of slave oscillators to a tunable master oscillator or to one of a number of master oscillators (of different frequencies). A disadvantage of the present design is that the lack of a high-Q resonator makes the (free-running) oscillation frequency difficult to predict exactly at the design stage. However, this could be overcome by incorporating limited electronic tuning (e.g. varactor control) into the design. The low-Q resonator will also cause increased phase noise and this needs to be examined in future work.

Finally, the effects of modulated locking signals on the oscillator have been investigated. Initial measurements have been made that demonstrate the use of wide-locking bandwidth oscillators as FM transmitters. It has also been shown that such oscillators can be used for AM-to-PM conversion.

Appendix
HPT Equivalent Circuit Parameters and Values

The HPT equivalent circuit parameters were calculated from the known device physics and behavior and then optimized employing *Touchstone* simulations and comparing with measurements.

Y_{21} is a modified form of the transconductance that takes into account the diffusion mechanism in the base [17]

$$Y_{21} = \frac{g_m}{1 + j\omega\tau_0}\left[\frac{1 - \exp(j\omega\tau_{cs})}{j\omega\tau_{cs}}\right]\exp(-j\omega(k\tau_0 + \tau_{bs})) \tag{A1}$$

where

τ_0 is the base diffusion time = 0.149 ps,
τ_{bs} is the base diffusion time = 0.149 ps,
k is a dimensionless constant = 0.127,

and the transconductance, g_m, and the collector base depletion layer transit time are in common with the other equivalent bias-dependent circuit parameters. These parameters are defined below and their optimized values at 8-mA collector-emitter bias current, I_{CE}, are also given in Table I.

The base-emitter depletion capacitance c_{je} is neglected as it is assumed to be much smaller than c_{be}. An emitter contact resistance, $r_{ee} = 0.2\ \Omega$, a collector contact resistance, $r_{cc} = 1\ \Omega$ and a parasitic bonding pad capacitance, $c_p = 0.1$ pF are assumed.

ACKNOWLEDGMENT

The HPT's were provided by BT Laboratories. The authors would like to thank Prof. P. A. Davies at the University of Kent and Dr. D. Wake at BT Labs. for useful discussions.

REFERENCES

[1] S. Meyer, J. Guena, J. C. Leost, E. Penard, and M. Goloubkoff, "A new concept of LANs: Passive microwave links hooked onto a fiber optic backbone," in *1993 IEEE MTT-S Int. Microwave Symp. Dig.*, Atlanta, GA, June 14–18, 1993, pp. 1549–1552.

[2] A. J. Cooper, "'Fibre/radio' for the provision of cordless/mobile telephony services in the access network," *Electron. Lett.*, vol. 26, pp. 2054–2056, 1990.

[3] M. Shibutani, T. Kanai, W. Domom, K. Emura, and J. Namiki, "Optical fiber feeder for microcellular mobile communication systems (H-015)," *IEEE J. Selected Areas Commun.*, vol. 11, pp. 1118–1126, 1993.

[4] W. S. Birkmayer and M. J. Wale, "Proof-of-concept model of a coherent optical beam-forming network," *IEE Proc.*, Optoelectronics, pt. J, vol. 139, pp. 301–304, 1992.

[5] E. H. Monsay, K. C. Baldwin, and M. J. Caccuitto, "Photonic true time delay for high-frequency phased array systems," *IEEE Photon. Technol. Lett.*, vol. 6, pp. 118–120, 1994.

[6] A. J. Seeds and J. R. Forrest, "Initial observations of optical injection locking of an X-band impatt oscillator," *Electron. Lett.*, vol. 14, pp. 829–830, 1978.

[7] A. Bangert and Th. Lauterbach, "Initial observations of optical injection locking of oscillators using heterojunction bipolar transistors," *Electron. Lett.*, vol. 28, pp. 621–623, 1992.

[8] A. Bangert, J. Rosenzweig, A. Huelsmann, G. Kaufel, K. Koehler, and J. Schneider, "Optical control of pseudomorphic HEMT-based MMIC oscillators," *Microwave and Optical Technol. Lett.*, vol. 6, pp. 36–38, 1993.

[9] M. Karakucuk, W. Q. Li, P. N. Freeman, J. R. East, G. I. Haddad, and P. K. Bhattacharya, "A direct optically injection-locked 2.6-GHz HBT oscillator," *Microwave and Optical Technol. Lett.*, vol. 6, pp. 609–611, 1993.

[10] T. P. Higgins, J. F. Harvey, D. J. Sturzebecher, A. C. Paolella, and R. A. Lux, "Direct optical frequency modulation and injection locking of resonant tunnel diode oscillator," *Electron. Lett.*, vol. 28, pp. 1574–1576, 1992.

[11] X. Zhang and A. S. Daryoush, "Full 360° phase shifting of injection-locked oscillators," *IEEE Microwave and Guided Wave Lett.*, vol. 3, pp. 14–16, 1993.

[12] R. D. Esman, L. Goldberg, and J. F. Weller, "Optical phase control of an optically injection-locked FET oscillator," *IEEE Trans. Microwave Theory Tech.*, vol. 37, pp. 1512–1518, 1989.

[13] I. D. Blanchflower and A. J. Seeds, "Optical control of frequency and phase of GaAs MESFET oscillator," *Electron. Lett.*, vol. 25, pp. 359–360, 1989.

[14] R. Adler, "A study of locking phenomena in oscillators," *Proc. IRE*, vol. 34, pp. 351–357, 1946.

[15] G. D. Vendelin, *Design of Amplifiers and Oscillators by the S-Parameter Method*. New York: Wiley, 1982.

[16] S. R. Cochran and S. Y. Wang, "Efficient optical injection locking of electronic oscillators," *Microwave J.*, May 1989, pp. 315–327.

[17] F. Ali and A. Gupta, *HEMTs and HBTs: Devices, Fabrication and Circuits*. Norwood MA: Artech House, 1991, ch. 4.

[18] J. C. Campbell, "Phototransistors for lightwave communications," in *Semiconductors and Semimetals*, R. K. Willardson and A. C. Beer, Eds. New York: Academic, 1985, vol. 22-D.

[19] D. Wake, D. J. Newson, M. J. Harlow, and I. D. Henning, "Optically biased, edge-coupled InP/InGaAs heterojunction phototransistors," *Electron. Lett.*, vol. 29, pp. 2217–2219, 1993.

[20] D. Sommer, N. J. Gomes, and D. Wake, "Optical injection locking of microstrip MESFET oscillator using heterojunction phototransistors," *Electron. Lett.*, vol. 30, pp. 1097–1098, 1994.

[21] T. Isobe and M. Tokida, "A new microwave amplifier for multichannel FM signals using a synchronized oscillator," *IEEE J. Solid-State Circuits*, vol. SC-4, pp. 400–408, 1969.

Dirk Sommer was born on May 25, 1969 in Heilbronn, Germany. Since 1990 he has studied electronic engineering specializing in communicationsat the Technical University of Darmstadt.

From 1993–1994 he spent six months carrying out project work in the Optical Communications Group at the University of Kent.

Nathan J. Gomes received the B.Sc. (Eng.) degree from the University of Sussex in 1984 and the Ph.D. degree from University College London in 1988.

He spent one year investigating the high-speed modulation properties of semiconductor lasers at ENST, Paris. Since late 1989 he has been a Lecturer in the Electronic Engineering Laboratories at the University of Kent, where he is a member of the Optical Communications Group. His current research interests are in high-speed and microwave/mm-wave optoelectronic devices and circuits.